SAND2015-1326C
Proceedings of the ASME 2015 34th International Conference on Ocean, Offshore and Arctic Engineering
OMAE2015
May 31-June 5, 2015, St. John's, Newfoundland, Canada

OMAE2015-41993

SENSITIVITY OF A WAVE ENERGY CONVERTER DYNAMICS MODEL TO NONLINEAR HYDROSTATIC MODELS

Ryan G. Coe*
Water Power Technologies Department
Sandia National Laboratories
Albuquerque, NM 87185
Email: Ryan.Coe@sandia.gov

Diana L. Bull
Water Power Technologies Department
Sandia National Laboratories
Albuquerque, NM 87185
Email: Diana.Bull@sandia.gov

ABSTRACT

A three dimensional time-domain model, based on Cummins equation, has been developed for an axisymmetric point absorbing wave energy converter (WEC) with an irregular cross section. This model incorporates a number of nonlinearities to accurately account for the dynamics of the device: hydrostatic restoring, motion constraints, saturation of the power-take-off force, and kinematic nonlinearities. Here, an interpolation model of the hydrostatic restoring reaction is developed and compared with a surface integral based method. The effects of these nonlinear hydrostatic models on device dynamics are explored by comparing predictions against those of a linear model. For the studied WEC, the interpolation model offers a large improvement over a linear model and is roughly two orders-of-magnitude less computationally expensive than the surface integral based method.

NOMENCLATURE

WEC Wave energy converter.
T3R2 "Three-translation, two-rotation" WEC studied here.
PCC Power-conversion-chain.
PMT Planar-motion-table.
$\mathbf{0}_{n\times n}$ Empty matrix of size n.
$\mathbf{A}_\infty$ Infinite added mass matrix for float.
$\mathbf{A}_r$, $\mathbf{B}_r$, $\mathbf{C}_r$ Radiation damping state-space system matrices.
$\mathbf{C}(\dot{\xi})$ Centripetal-Coriolis matrix.
$\mathbf{C}_m$ Linear mooring matrix.
$\mathbf{G}$ Linear hydrostatic matrix.
$\mathbf{I}_{RB}$ Rigid-body moments of inertia.
$\mathbf{I}_{n\times n}$ Identity matrix of size n.
$\mathbf{J}(\vartheta)$ Euler angle transformation matrix .
$\dot{\mathbf{J}}(\vartheta)$ Time derivative of Euler angle transformation matrix.
$\mathbf{K}_r$ Radiation damping kernel matrix.
$\mathbf{M}_{RB}$ Rigid-body inertia matrix for float.
$\mathbf{M}_{PCC}$ Rigid-body inertia matrix for power-conversion-chain.
$\mathbf{M}_{PMT}$ Rigid-body inertia matrix for planar-motion-table.
$\mathbf{S}(\lambda)$ Skew symmetric matrix of the vector λ.
A_{wp} Area of the waterplane.
g Gravitational acceleration.
H_s Significant wave height.
r_G Center of gravity location ($r_G = \left[x_G\ y_G\ z_G\right]^{\mathrm{T}}$).
S_{ii} 2^{nd}-moments of the waterplane area.
T_p Peak period.
η Inertial position and orientation ($\eta = \left[x\ y\ z\ \phi\ \theta\ \psi\right]^{\mathrm{T}}$).
μ Radiation damping reaction.
ρ Fluid density.
τ_h Hydrostatic reaction ($\tau_h = \left[f_h\ m_h\right]^{\mathrm{T}}$).
τ_v Viscous damping vector.
τ_e Excitation vector.
τ_u Control input vector.
$\forall$ Submerged volume.
$\dot{\xi}$ Body-fixed velocity ($\dot{\xi} = \left[u\ v\ w\ p\ q\ r\right]^{\mathrm{T}}$).
ζ Free surface elevation.

*Address all correspondence to this author.

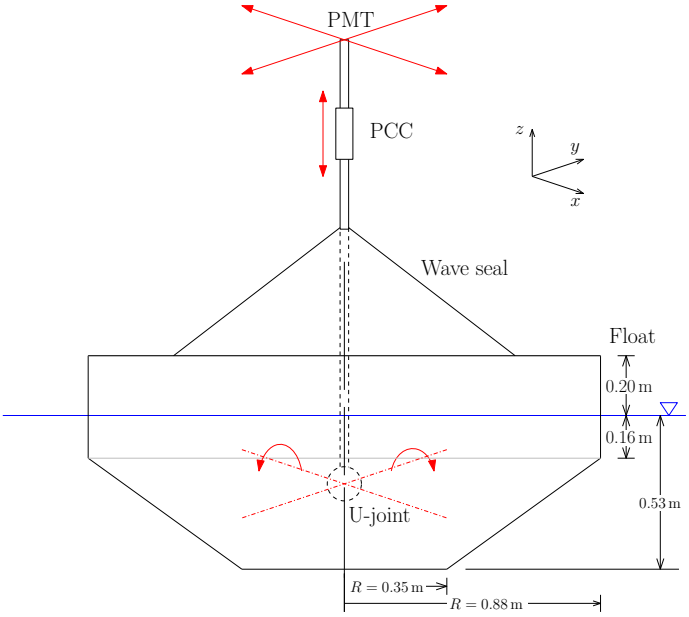

Figure 1. T3R2 EXPERIMENTAL WEC DESIGN.

INTRODUCTION

A WEC dynamics model, an earlier version of which was described in [1], is currently being developed to support a research effort focused on the development and testing of advanced WEC control strategies. This project will employ a purpose-designed WEC, intended to provide insight into the effectiveness of prospective control strategies. A cartoon of this WEC with dimensions is shown in Fig. 1. This device, referred to as the T3R2 ("three-translations, two rotations") will be tested and evaluated at model-scale.

METHODOLOGY

A model based on the formulation suggested by Cummins [2] has been developed for the T3R2. This model follows the same general framework as that discussed in [1]. This paper will focus on improvements made to that model.

$$\begin{aligned}&\left[\mathbf{M}_{RB}+\mathbf{A}_{\infty}+\mathbf{J}^{\mathrm{T}}(\vartheta)\left(\mathbf{M}_{PCC}+\mathbf{M}_{PMT}\right)\mathbf{J}^{-1}(\vartheta)\right]\ddot{\xi}\\&+\left[\mathbf{J}^{\mathrm{T}}(\vartheta)\left(\mathbf{M}_{PCC}+\mathbf{M}_{PMT}\right)\dot{\mathbf{J}}\left(\vartheta,\dot{\vartheta}\right)+\mathbf{C}(\dot{\xi})\right]\dot{\xi}\\&+\int_0^t\mathbf{K}_r(t-\lambda)\dot{\xi}(\lambda)\,d\lambda\\&+\mathbf{J}(\vartheta)^{\mathrm{T}}(\tau_h+\mathbf{C}_m\eta)+\tau_v=\tau_e+\tau_u.\end{aligned}\tag{1}$$

Kinematics

Two coordinate systems are used to describe the dynamics of the T3R2 in (1): the inertial position, η, and the body-fixed velocity, $\dot{\xi}$.[1]

$$\eta=\left[\varepsilon\ \vartheta\right]^{\mathrm{T}}=\left[x\ y\ z\ \phi\ \theta\ \psi\right]^{\mathrm{T}}\tag{2a}$$

$$\dot{\xi}=\left[\dot{\xi}_1\ \dot{\xi}_2\right]^{\mathrm{T}}=\left[u\ v\ w\ p\ q\ r\right]^{\mathrm{T}}\tag{2b}$$

The orientation of the inertial coordinate system is illustrated in Fig. 1 (this is also the initial orientation of the body-fixed coordinate system). Euler-angle transformation matrices (see e.g., [1, 3]) can be employed to couple these two systems. The dynamics of the two frames can be equated as follows.

$$\dot{\eta}=\mathbf{J}(\vartheta)\dot{\xi}\tag{3a}$$

$$\ddot{\eta}=\dot{\mathbf{J}}(\vartheta,\dot{\vartheta})\dot{\xi}+\mathbf{J}(\vartheta)\ddot{\xi}\tag{3b}$$

The forces and moments in each frame are related through a similar relationship.

$$\tau_{\eta}=\mathbf{J}^{-\mathrm{T}}(\vartheta)\tau_{\dot{\xi}}\tag{4}$$

Here, τ_{η} and $\tau_{\dot{\xi}}$ indicate the forces and moments acting on the body in inertial and body-fixed reference frames respectively. The Euler-angle transformation matrix employed in these relationships is

$$\mathbf{J}=\begin{bmatrix}\mathbf{R}(\vartheta)&\mathbf{0}_{3\times3}\\\mathbf{0}_{3\times3}&\mathbf{T}(\vartheta)\end{bmatrix}.\tag{5}$$

For the T3R2, as no rotation occurs about the vertical axis ($\psi=0$), the component blocks of (5) are

$$\mathbf{R}(\vartheta)=\begin{bmatrix}c\theta&s\theta s\phi&c\phi s\theta\\0&c\phi&-s\phi\\-s\theta&c\theta s\phi&c\theta c\phi\end{bmatrix}\tag{6a}$$

$$\mathbf{T}(\vartheta)=\begin{bmatrix}1&s\phi t\theta&c\phi t\theta\\0&c\phi&-s\phi\\0&s\phi/c\theta&c\phi/c\theta\end{bmatrix}.\tag{6b}$$

[1] Note that $\int\dot{\xi}\,dt$ has no meaning, as the orientation of body is always changing.

The time-derivative of transformation matrix, $\dot{\mathbf{J}}(\vartheta, \dot{\vartheta})$, required by (3b) can be obtained by setting $\phi = \phi(t)$ and $\theta = \theta(t)$ and differentiating with respect to t.

Inertial Effects

The rigid-body inertia of the float is described by the symmetric matrix $\mathbf{M}_{RB}$.

$$\mathbf{M}_{RB} = \begin{bmatrix} m_{float}\mathbf{I}_{3\times 3} & -m_{float}\mathbf{S}(r_G) \\ m_{float}\mathbf{S}(r_G) & \mathbf{I}_{RB} \end{bmatrix} \tag{7}$$

Here, the skew-symmetric matrix operator is employed. The skew-symmetric matrix for an arbitrary vector $\vec{\lambda} = \begin{bmatrix}\lambda_1 & \lambda_2 & \lambda_3\end{bmatrix}^{\mathrm{T}}$ is defined as

$$\mathbf{S}(\lambda) = \begin{bmatrix} 0 & -\lambda_3 & \lambda_2 \\ \lambda_3 & 0 & -\lambda_1 \\ -\lambda_2 & \lambda_1 & 0 \end{bmatrix}. \tag{8}$$

Centripetal-Coriolis effects, due to the use of a non-inertial reference frame in the Newton-Euler equation (1), are given for the two mass matrices which rotate with the float ($\mathbf{M}_{RB}$ and $\mathbf{A}_\infty$) as [3]

$$\mathbf{C}(\dot{\xi}) = \begin{bmatrix} \mathbf{0}_{3\times 3} & -\mathbf{S}(\mathbf{M}_{11}\dot{\xi}_1 + \mathbf{M}_{12}\dot{\xi}_2) \\ -\mathbf{S}(\mathbf{M}_{11}\dot{\xi}_1 + \mathbf{M}_{12}\dot{\xi}_2) & -\mathbf{S}(\mathbf{M}_{21}\dot{\xi}_1 + \mathbf{M}_{22}\dot{\xi}_2) \end{bmatrix}. \tag{9}$$

Here, the 6×6 mass matrix has been defined by 3×3 quadrants (e.g., $\mathbf{M}_{11}$ is the upper left quadrant).

The rigid-body inertia of the PCC and PMT is represented in a similar manner, however, these members only affect translation modes of motion, as the PCC and PMT are not allowed to rotate. In the process of including these inertial effects in the equations of motion, which are written in the body-fixed frame, (3b) produces both the inertial term on the first line of (1) and the first term in the second line of (1).

Radiation

As discussed in [1], the radiation reaction, $\mu(t)$, can be represented by a state-space model (SSM) to partially alleviate the computational burden imposed by the convolution in (1).

$$\begin{aligned} \dot{x}_r &= \mathbf{A_r} x_r + \mathbf{B_r}\dot{\xi}(t) \\ \breve{\mu}(t) &= \mathbf{C_r} x_r \end{aligned} \tag{10}$$
$$\text{such that } \breve{\mu}(t) \approx \mu = \int_0^t \mathbf{K}_r(t-\lambda)\dot{\xi}(\lambda)\, d\lambda$$

An SSM to represent the IRF for a given mode can be obtained in either the time or frequency domain (see e.g., [4]). The full six degree-of-freedom radiation effects can be combined by assembling a compound SSM [1].

Hydrostatics

Three models were developed to represent the hydrostatic/gravitational reaction on the T3R2's float: a linear model, a surface integral based model and an interpolation based model (which is informed by the surface integral model).

Linear Formulation. Quite often, a linear formulation is used to represent the hydrostatic/gravitational reaction for a floating body (see e.g. [5]). As is generally the case, if the center of gravity and center of buoyancy lie on the same vertical line (i.e. the body is statically stable), the linear hydrostatic coefficient matrix $\mathbf{G}$ is a sparse diagonal 6×6 matrix with

$$\mathbf{G}_{33} = \rho g A_{wp} \tag{11a}$$
$$\mathbf{G}_{44} = \rho g \forall \left(\frac{S_{22}}{\forall} + z_B - z_G \right) \tag{11b}$$
$$\mathbf{G}_{55} = \rho g \forall \left(\frac{S_{11}}{\forall} + z_B - z_G \right). \tag{11c}$$

This linear assumption is valid for vertical motions in which the body is "wall-side" (i.e. the waterplane does not change as a function of draft) and for small rotational motions.

Surface Integral Formulation. The buoyancy force experienced by a submerged or partially submerged body is due to the hydrostatic pressure that acts on its surface. Assuming a constant density, the hydrostatic pressure in a water column increases linearly with depth.

$$\frac{\partial p}{\partial z} = -\rho g \tag{12}$$

The hydrostatic pressure can be integrated over the surface of a body to obtain the total hydrostatic force.

$$f_H = -\rho g \int_A z \cdot \hat{n}\, dA \tag{13}$$

For a body comprised of a finite set of q flat faces, each with an area of A_j and unit normal vector of $\hat{n}_j$, (13) can be written as

$$f_H = -\rho g \sum_j^q z_j A_j \cdot \hat{n}_j. \tag{14}$$

Similarly, the moment on the body, about a point to which each discrete surface has a vector r_j, is given by

$$m_H = -\rho g \sum_j^q z_j A_j \cdot (r_j \times \hat{n}_j). \tag{15}$$

The hydrostatic reaction on the body can thus be determined at each time-step in a simulation via (14) and (15), while taking account for the instantaneous submerged geometry. In this study, the submerged geometry was determined from the instantaneous body position, η, but did not consider the instantaneous free surface position (i.e. for the purposes of the hydrostatic reaction calculations, $\zeta(t,x,y) = 0$). The impact of including this dependency will be considered in future work.

These calculation can be implemented numerically via a triangulated description of the body's surface. Here, the popular STL (STereoLithograph) CAD format was employed. Figure 2 shows the geometry used to represent the T3R2 (pitched at an orientation of $\theta = 25°$) and pressure distribution resulting from the hydrostatic calculations.[2]

Two verification studies, the results of which are both shown in Fig. 3, were conducted for the surface integral hydrostatic model:

1. *Buoyancy force on a sphere at varying drafts* - A sphere with a radius of 1 m, was analyzed at a range of drafts ($0 \leq T \leq 2r$); the computed vertical buoyancy forces are compared in Fig. 3a to the analytic solution via the expression for the volume of a spherical cap.

$$\begin{aligned} \forall(T) &= \frac{\pi}{3} T^2 (3r - T) \\ \tau_h(3) &= \forall(T)\rho g \end{aligned} \tag{16}$$

[2]Note that the CAD geometry used for the nonlinear hydrostatics does not replicate the geometry of the T3R2's "Wave seal" (see Fig. 1).

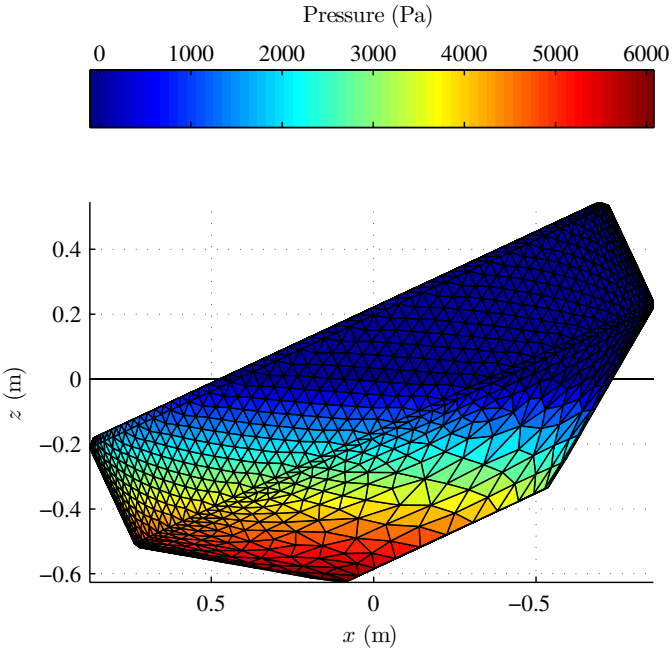

Figure 2. TRIANGULATED T3R2 GEOMETRY AND RESULTING HYDROSTATIC PRESSURE DISTRIBUTION, PITCHED AT AN ORIENTATION OF $\theta = 25°$.

2. *Buoyancy force on a block at varying angles of pitch* - A rectangular block ($1 \times 0.5 \times 0.25$ m, nominally floating with a draft of 0.125 m, a length of 1 m and a beam of 0.5 m; the center of gravity located at the center of block's "keel") was analyzed at varying angles of pitch; the pitch restoring moment calculated via (15) is compared the a linear model (11c) in Fig. 3b .

Linear Interpolation Formulation. By evaluating the surface integral hydrostatic model for a matrix of drafts ($z_{min} \leq z \leq z_{max}$) and pitch angles ($\theta_{min} \leq \theta \leq \theta_{max}$), response surfaces can be populated and used in a two-dimensional linear interpolation scheme (in this case, MATLAB's 'linearinterp' scheme was employed [6]). In use, this interpolation model is roughly 300 times faster than the surface integral hydrostatic model. (Note that, as the T3R2 is axisymmetric, the roll and pitch reactions have the same parametric shape.) Figure 4 shows the surfaces to represent the heave and pitch hydrostatic reactions. Here, the heave force and pitching moment are shown as they appear in (1) as τ_h (i.e. the sign of the reaction is consistent with the location of this term on the left-hand side of the equation). By comparing Figs. 4a and 4b, we can see that, for the T3R2, the heave restoring reaction is primarily dependent on the vertical position,

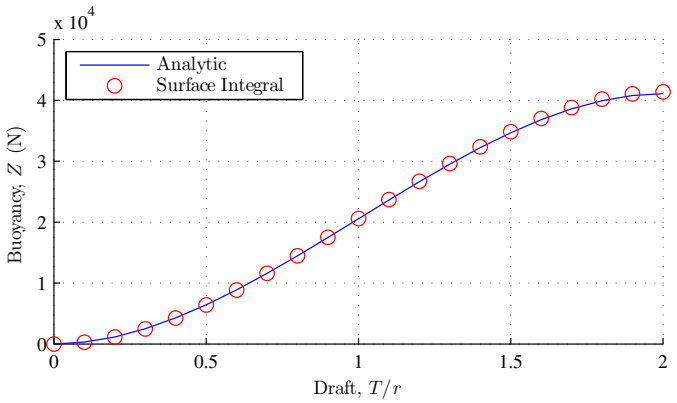

(a) BUOYANCY FORCE ON A SPHERE AT VARYING DRAFTS.

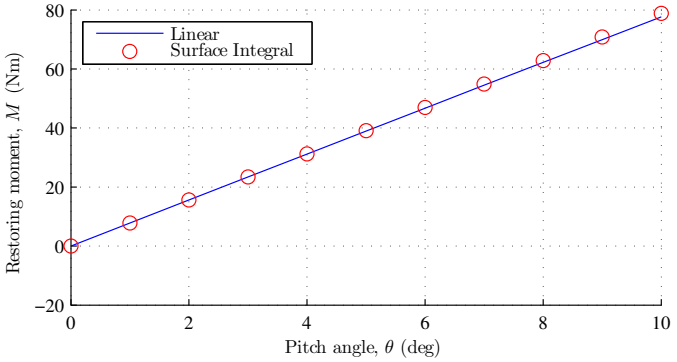

(b) RESTORING MOMENT ON A BLOCK AT VARYING ANGLES OF PITCH.

Figure 3. VERIFICATION STUDIES FOR SURFACE INTEGRAL HYDROSTATIC MODEL.

while the pitch restoring reaction shows similar magnitudes of influence from the pitch and vertical position.

The nonlinearity of these reactions, and its dependency on the displacement magnitude, is also illustrated in Fig. 5. Here, the heave and pitch restoring reaction prediction from each hydrostatic model is a shown for a range of displacements (the surface integral and interpolation result are shown together here, as they overlap very closely). The T3R2 float becomes submerged at a position of $z \leq -0.2\,\text{m}$; this is visible in Fig. 5a where at $z = -0.2\,\text{m}$ the integral/interpolation hydrostatic reaction levels off as the body becomes fully submerged (this behavior is uncaptured by the linear model). The pitch reaction, shown in Fig. 5b, exhibits a more gradually-acting nonlinearity.

RESULTS

Free Decay

Decay tests were conducted, in both heave and pitch, to assess the effect of employing the nonlinear (instantaneous) buoy-

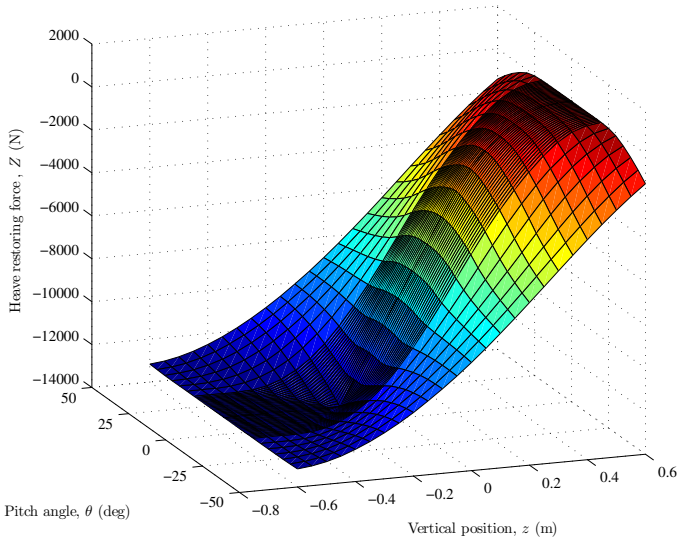

(a) HEAVE

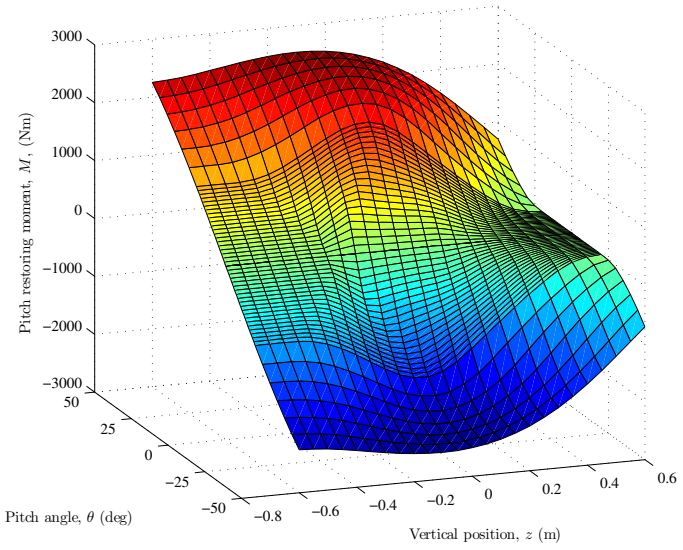

(b) PITCH

Figure 4. SURFACES FOR HEAVE AND PITCH REACTIONS.

ancy models. Figure 6 summarizes the results for decay in heave. Figure 6a shows the decay time histories for a range of different initial offsets. Predictions from the linear model (which are the same for all motion amplitudes) are shown with those from the surface integral and interpolation methods (which are shown together as they match closely). As expected, the nonlinear model's prediction can be seen to approach the linear model as the initial offset (and therefore motion amplitude) decreases. Figure 6b shows a summary of these results by plotting the natural frequencies observed for each of these tests. In analyzing these results, it is helpful to refer to the geometric description of

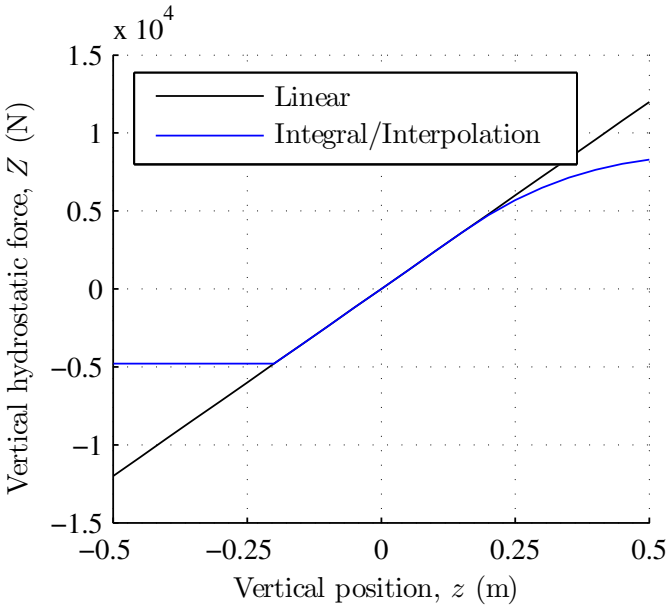

(a) HEAVE

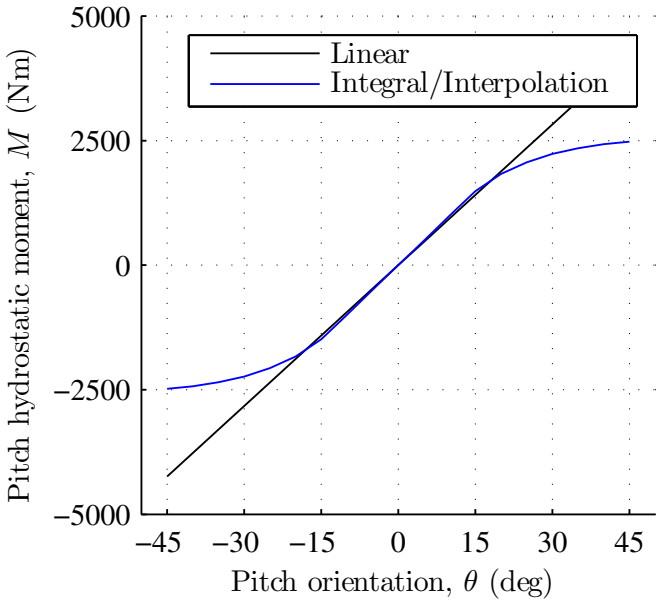

(b) PITCH

Figure 5. COMPARISON OF PREDICTED REACTIONS FROM LINEAR AND SURFACE INTEGRAL/INTERPOLATION HYDROSTATIC RESTORING MODELS.

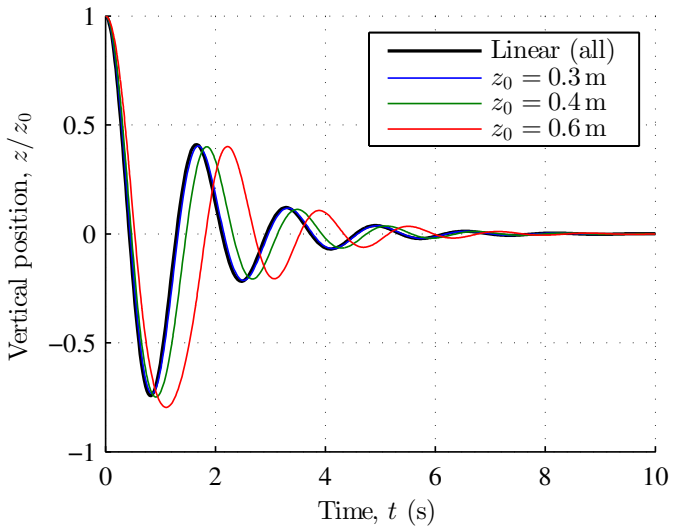

(a) NORMALIZED TIME-HISTORIES FOR LINEAR (BLACK) AND SURFACE INTEGRAL/INTERPOLATION HYDROSTATIC FORMULATIONS.

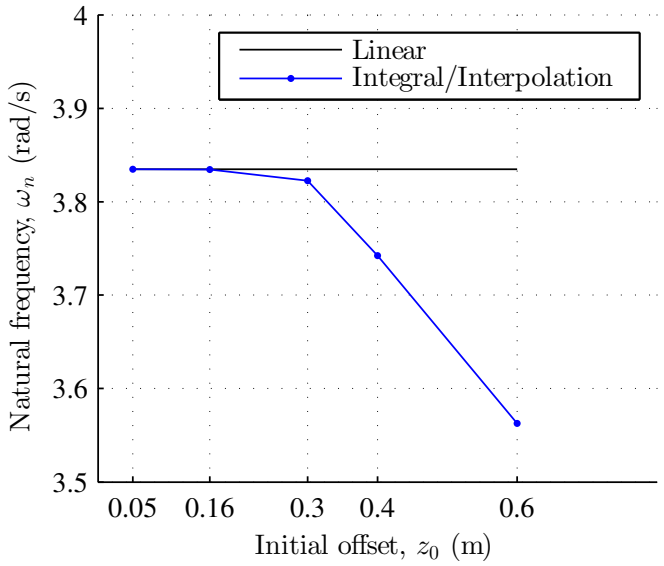

(b) NATURAL FREQUENCIES.

Figure 6. HEAVE DECAY PREDICTION FROM DIFFERENT HYDROSTATIC FORMULATIONS WITH A RANGE OF INITIAL OFFSETS.

the T3R2 float shown in Fig. 1. We can see that the T3R2 float is wall-sided for $-0.16 \leq z \leq 0.20$ m; within this range, the linear and nonlinear models match well, whereas outside of this range the discrepancy between them grows.

Figure 7 shows a similar analysis for the pitch decay of the T3R2. Here, it is not quite as straight forward to understand where the nonlinear behavior "should" arise. However, looking at Fig. 5b, the nonlinear models can be seen to show a substantial difference from the linear model near an orientation of $\sim 20°$. This behavior agrees well with the results shown in Fig. 7.

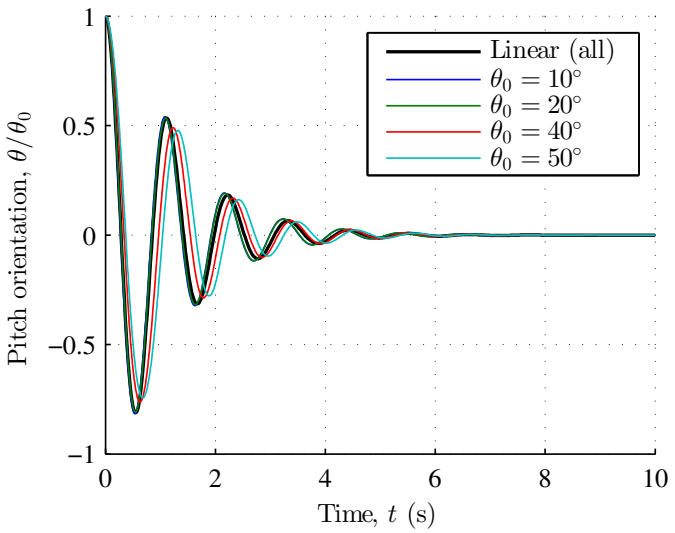

(a) NORMALIZED TIME-HISTORIES FOR LINEAR (BLACK) AND SURFACE INTEGRAL/INTERPOLATION HYDROSTATIC FORMULATIONS.

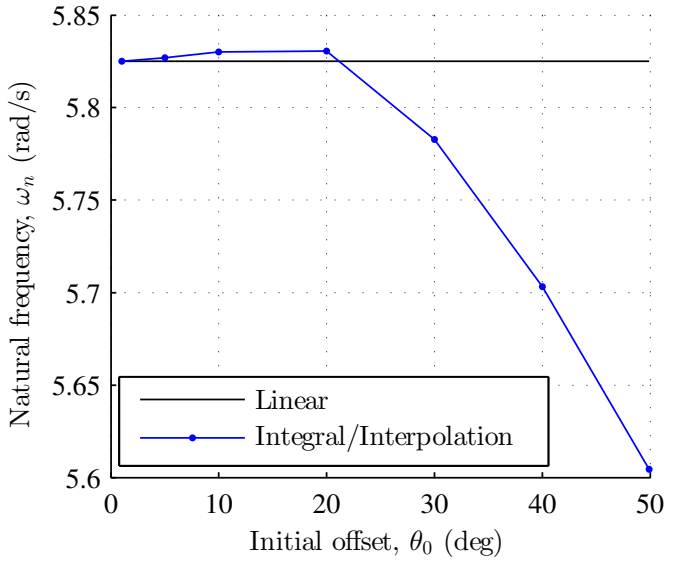

(b) NATURAL FREQUENCIES.

Figure 7. PITCH DECAY PREDICTION FROM DIFFERENT HYDROSTATIC FORMULATIONS WITH A RANGE OF INITIAL OFFSETS.

Irregular Sea State Response

A set of four of simulations were performed to qualitatively assess the sensitivity of model predictions to the nonlinear hydrostatic models. Two waves, with significant wave heights of H_s and peak periods of T_p were considered:

Wave A: $H_s = 0.20\,\text{m}$, $T_p = 1.4\,\text{s}$

Wave B: $H_s = 0.75\,\text{m}$, $T_p = 1.4\,\text{s}$

Figures 8 and 9 show the free surface time history and the response of the float for Wave A and Wave B respectively. In each case, float response predictions are shown for the linear hydrostatic model and the integral/interpolation hydrostatic model.

In Wave A, the two models predict very similar time-histories, with the greatest differences seen in pitch. Looking at the magnitude of the motion, we can see that the float remains within its wall-sided region ($-0.16 \leq z \leq 0.20\,\text{m}$), and the dynamics should therefore be mostly-linear. The small difference seen between the vertical position histories in Fig. 8 is likely due to nonlinear kinematic coupling with the pitch motion (note that heave couples into axial position via nonlinear kinematics).

For Wave B (see Fig. 9), the amplitude of the float's motion is much larger. This larger motion introduces substantial nonlinearity to the vertical hydrostatic force and therefore the dynamics in that mode. This can be seen in all three modes of motion.

CONLCUSIONS

A WEC dynamics modeling, based on Cummins' equation, has been formulated to model the nonlinear hydrostatic phenomena of a floating body. To study the effects of this nonlinearity, tests were conducted to study the decay responses and irregular wave responses of a single device with and without the nonlinear hydrostatic effects. The results show that, for the T3R2 device studied here, the nonlinear model can have a substantial effect on the dynamics of the device. However, if the vertical motion is the primary concern, the nonlinear effects are not great when the motion of the device is small enough to remain within the wall-sided region.

As discussed in the Methodology section of this paper, future work with the model developed here will investigate the effect of using the instantaneous free surface position in determining the submerged geometry of the body. Additionally, a major caveat to the irregular wave response results shown here is linked to the influence of the hydrostatic model on the float's position in the horizontal plane. In the current model, the excitation reaction is not based on the position of the float which does not reflect reality ($\zeta = f(x,y,t)$). The nonlinear hydrostatic models' effect on the float's position would likely create even larger differences in the vertical position were the position dependence of excitation taken into account.

ACKNOWLEDGMENT

This work was funded by the U.S. Department of Energy's Wind and Water Power Technologies Office. Sandia National Laboratories is a multi-program laboratory managed and operated by Sandia Corporation, a wholly owned subsidiary of Lockheed Martin Corporation, for the U.S. Department of Energy's National Nuclear Security Administration under contract DE-AC04-94AL85000.

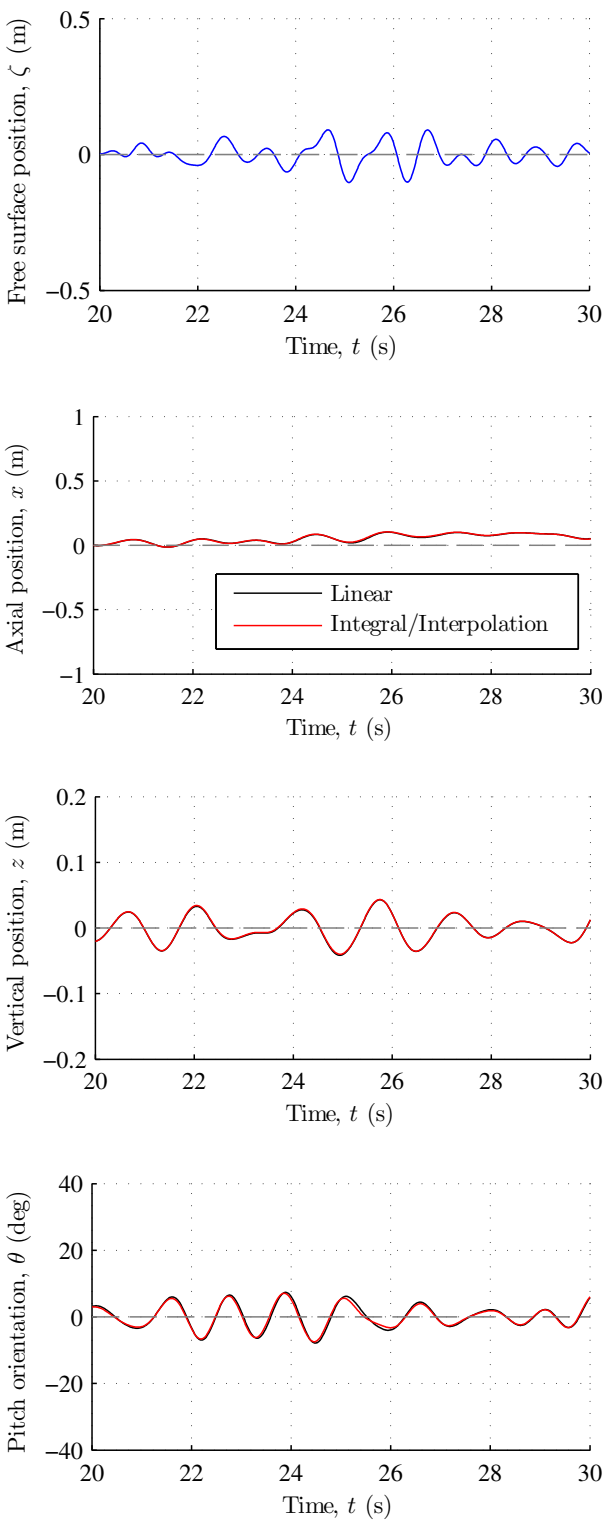

Figure 8. T3R2 RESPONSE IN IRREGULAR WAVES WITH LINEAR AND NONLINEAR HYDROSTATIC MODELS ($H_s = 0.2\,\text{m}$, $T_p = 1.4\,\text{s}$).

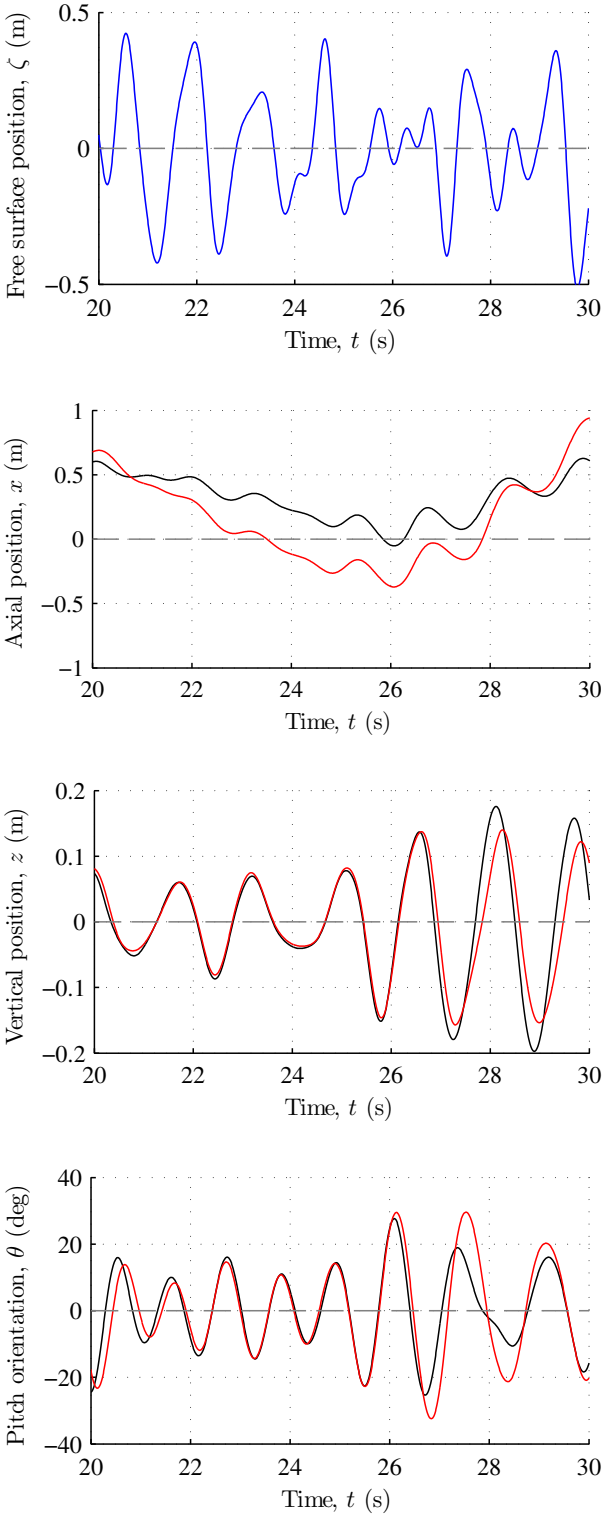

Figure 9. T3R2 RESPONSE IN IRREGULAR WAVES WITH LINEAR AND NONLINEAR HYDROSTATIC MODELS ($H_s = 0.75\,\text{m}$, $T_p = 1.4\,\text{s}$). (NOTE: FIG. 9 USES LEGEND SHOWN IN FIG. 8)

REFERENCES

[1] Coe, R. G., and Bull, D. L., 2014. "Nonlinear time-domain performance model for a wave energy converter in three dimensions". In OCEANS2014, IEEE.

[2] Cummins, W. E., 1962. The impulse response function and ship motions. Tech. Rep. DTNSDRC 1661, Department of the Navy, David Taylor Model Basin, Bethesda, MD.

[3] Fossen, T. I., 1994. *Guidance and control of ocean vehicles*. Wiley, Chichester; New York.

[4] Perez, T., and Fossen, T. I., 2008. "Time- vs. frequency-domain identification of parametric radiation force models for marine structures at zero speed". *Modeling, Identification and Control,* ***29***(1), p. 119.

[5] Newman, J. N., 1978. *Marine hydrodynamics*. MIT Press, Cambridge, Massachusetts.

[6] MATLAB, 2013. *8.1.0.604 (R2013a)*. The MathWorks Inc., Natick, Massachusetts.